Third International Conference on CFD in the Minerals and Process Industries
CSIRO, Melbourne, Australia
10-12 December 2003

CFD MODELLING OF THE HEAT AND MASS TRANSFER PROCESS DURING THE EVAPORATION OF WATER FROM A CIRCULAR CYLINDER

Francisco Javier TRUJILLO[1], Simon J. LOVATT[2], Mark B. HARRIS[2], Jim WILLIX[2], and Q. Tuan PHAM[1]

[1] *School of Chemical engineering and Industrial Chemistry,* University of New South Wales, Sydney 2052, Australia

[2] AgResearch MIRINZ Centre Private Bag 3123, Hamilton, New Zealand

ABSTRACT

The purpose of this work is to simulate the heat and mass transfer during the evaporation of water from a cylinder at moderate Reynolds numbers. The process was modelled on FLUENT 6.1.18 and the results were compared with experimental data. Different mathematical approaches were used to assess which model fit the data better. Four turbulent models were used and compared: the laminar, standard κ-ε, RNG κ-ε and the SST κ-ω. Two wall treatment approaches were followed: the standard wall function and the enhanced wall treatment. The model that best fits the experimental data was the RNG κ-ε model using the enhanced wall treatment and taking in account the effect of radiation. This model was able to predict the changes of temperature around the cylinders as well as the heat (h) and mass (h_m) transfer coefficients. The ratio between h and h_m was calculated with the CFD modelling, showing that this ratio is not constant at low air velocities reaching a minimum of up to 19% of difference, at the point of separation of the boundary layer, comparing with the Chilton-Colburn analogy. It was found that this difference may be caused by the heat of radiation that becomes important at low Reynolds numbers.

NOMENCLATURE

C_P	Heat capacity
C_μ	RNG κ-ε model constant
D	Diffusivity of water in air
ds	distance from node face to node cell
E	Empirical Constant
ε	Radiation emissivity
h	Local convective heat transfer coefficient
h_m	Local mass transfer coefficient
κ	Von Karman constant
L_e	Lewis number
J_w	Local mass flux on the wall
L_{vap}	Vaporization heat of water
P_c	Number function of Sc and Sc_t
RH	Relative Humidity (%)
Sc	Schmidt number
T	Temperature
$\dot{q}_w$	Wall heat flux
Y	Mass weigh composition
Y^*	Non-dimensional water composition on the near wall cell
y^*	Non-dimensional distance to the wall
y^+	Non-dimensional distance to the wall
y_C^*	Mass sub-layer thickness
μ	Dynamic viscosity
ρ	Density
σ	Stefan-Boltzmann constant
$\bar{x}$	Overall or global value of x

Subindices

a	Air
c	Cell
eff	Effective value
mol	Molecular value
t	Turbulent
w	Wall

INTRODUCTION

Heat and mass transfer between air and food products are involved in many food processing operations, such as freezing, drying and chilling. To control and optimize these processes, it is necessary to accurately know the local heat and mass transfer coefficients. They also determine the local temperature and surface water activity, which are two of the most important properties in the control of the bacterial growth.

Industrial meat chilling operations use low air velocities but may have high turbulence intensity. Due to the complex shape of the product, the boundary layer changes rapidly along the surface affecting the local heat and mass transfer coefficients. A circular cylinder under cross flow conditions was used to experimentally determine and model the heat and mass transfer coefficients. The air velocities used were 0.5, 1.5 and 3 m/s and a turbulence intensity of 2%.

EXPERIMENT PROCEDURE

Kondjoyan and Daudin's (1993b) approach of using a steady-state technique to estimate average surface heat and mass transfer coefficients was followed. Two wet plaster samples were placed into a wind tunnel (one for temperature measurement, one for weight measurement) and held under constant air conditions. Plaster samples were used, as it was claimed that the plaster surface remained fully wet for long periods of time. When steady state was reached, the heat extracted from the sample by

evaporation was balanced by that provided from the air stream through convection and radiation to the surface. Under these conditions, the surface of the sample approached the wet-bulb temperature of the air. The average sample heat and mass transfer coefficients were then computed based on the average surface temperature and the rate of evaporation (weight loss) measured from the samples.

The apparatus used comprised a 100mm diameter plaster cylinder, with a length also of 100mm. To reduce aerodynamic edge effects the plaster cylinder was located between two extra wet plasters as it seems in figure 1.

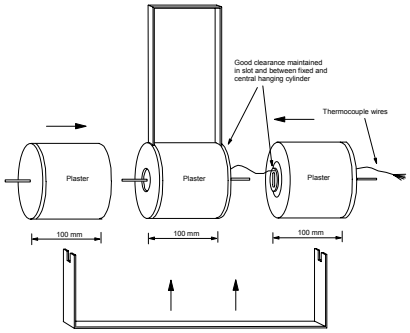

Figure 1: Experimental apparatus to minimise aerodynamic, heat and mass transfer edge effects.

The two plaster assemblies were hung in a controlled environment wind tunnel. One of the samples was weighed during the weight loss experiment, while the other had T type thermocouples inserted near the surface of the plaster to measure the surface temperature (Figure 2). Thus, any influence of the thermocouple wires on sample weight measurement was reduced.

During drying experiments, the air stream temperature, humidity and velocity were maintained at constant pre-determined levels. Plaster surface temperatures, air stream temperature, humidity, and sample weight were recorded versus time. At the start of each run, the plaster surface temperature took a little time to reach a steady state temperature distribution. This value was within 0.2 – 1.8 degrees of the wet bulb temperature, depending on the air velocity over the cylinder. Once this steady temperature was achieved, the rate of evaporation from the cylinder surface remained steady until most of the water in the plaster had evaporated (constant rate dying). After this point the surface temperatures would begin to rise, as mass transfer within the plaster began to limit the drying rate. The recorded data used was that obtained during the steady state stage.

This method has been used before to determine local heat and mass transfer coefficients on elliptical cylinders (Kondjoyan and Daudin's (1993a)) and at the surface of a pork hindquarter (Kondjoyan and Daudin's (1997)).

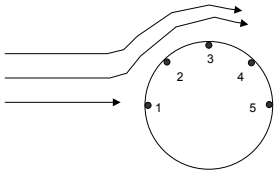

Figure 2: Thermocouples inserted just below the surface of the cylinder.

Calculation of experimental heat and mass transfer coefficient

A heat balance over the surface of the plaster during the constant rate drying period may be written:

$$h_m L_{vap}\left(Y_a - Y_w\right) + \varepsilon\sigma\left(T_a^4 - T_w^4\right) = h\left(T_w - T_a\right) \quad (1)$$

and the rate of mass transfer from the surface, J_w, as

$$J_w = h_m\left(Y_a - Y_w\right) \quad (2)$$

Rearranging these equations and integrating them over the surface of the plaster cylinder enables the overall heat and mass transfer coefficients to be calculated from measurements of the rate of weight loss, the plaster surface temperatures, air stream temperature and humidity:

$$\overline{h}_m = \frac{\overline{J}_w}{\left(Y_a - \overline{Y_w}\right)} \quad (3)$$

$$\overline{h} = \frac{-M_m L_{vap}}{\left(T_a - \overline{T_w}\right)} - \frac{\varepsilon\sigma\left(T_a^4 - \overline{T_w^4}\right)}{\left(T_a - \overline{T_w}\right)} \quad (4)$$

These equations incorporate some small spatial averaging errors. However, these errors were shown to be relatively insignificant by Kondjoyan and Daudin (<3% effect on h and h_m).

The mass transfer coefficients can also be calculated from the heat transfer coefficient if the relationship between heat and mass transfer is known. For laminar flow over flat plates it can be shown that:

$$\frac{h}{h_m} = C_P L_e^{2/3} \quad (5)$$

According to Lewis (1971) Equation 5 may be used to predict heat transfer values from mass transfer measurement. The error involved is much less than the deviation caused by such factors as free stream turbulence and wind tunnel blockage. Kestin and Wood (1971) used equation 5 to calculate the wall temperature and local mass transfer coefficient before and after the detachment of the boundary layer. This relationship (Chilton-Colburn analogy) has also been shown to hold for more complicated boundary layer flows including turbulent flow over a flat plate, laminar and turbulent flow over cylinders.

Introducing the variable, K, representing the ratio of heat to mass transfer:

$$K = \frac{h}{h_m L_{vap}} = \frac{\overline{h}}{\overline{h_m} L_{vap}} \quad (6)$$

the local heat and mass transfer coefficients may be calculated directly from the surface temperature measurements as:

$$h = \frac{\varepsilon\sigma\left(T_a^4 - T_w^4\right)}{\left[\left(T_w - T_a\right) + \left(Y_w - Y_a\right)/K\right]} \quad (7)$$

and

$$h_m = \frac{\varepsilon\sigma\left(T_a^4 - T_w^4\right)}{L_{vap}\left[K\left(T_w - T_a\right) + \left(Y_w - Y_a\right)\right]} \quad (8)$$

where Y_w can be calculated from the saturation curve knowing the local temperature.

MATHEMATICAL MODEL

Four mathematical models were used to calculate the turbulence and two different approaches were followed to solve the wall. The continuity, velocity, energy, moisture content, and additional turbulent transport equations were solved using FLUENT 6.1.18. The used turbulent models are:

1) Standard κ-ε model: it is a semi-empirical method based on the transport equation for turbulent kinetic energy (κ) and its dissipation rate (ε) (Launder and Spalding, 1974). This model was developed assuming that the flow is fully turbulent and the effects of molecular viscosity are negligible.

2) The RNG- κ-ε model: This model is derived from the Navier-Stokes equations using the "renormalization group" method that results in a model with constants different from those in the standard κ-ε model. It also results in a differential equation for turbulent viscosity that is integrated to obtain an accurate description of how the effective turbulent viscosity varies with the effective Reynolds number, allowing the model to better handle low-Reynolds number and near wall flows. Another advantage of this model is that it calculates the effective inverse Prandtl number (or Smith in the case of mass transfer) as a function of μ_{mol}/μ_{eff}, which is consistent with experimental evidence and allows heat and mass transfer to be calculated in low Reynolds number regions (Fluent Inc. (2003)).

3) The SST κ-ω model: it is an improved version of the standard κ-ω model based on model transport equations for the turbulence kinetic energy (κ) and the vorticity fluctuation of turbulence (ω). This model was designed to be applied throughout the boundary layer, provided that the near-wall mesh resolution is sufficient.

4) Laminar model: It assumes that the flow is laminar and it does not take into account turbulent effects.

Two wall treatment approaches were used:

1) Enhanced wall treatment (EWT): It is a near-wall modelling method that combines a two-layer model (the viscosity affected near wall region is completely resolved all the way to the viscous sub-layer) together with enhanced wall functions. The near-wall mesh created was fine enough to resolve down to the laminar sub-layer ($y^+ \approx 1$); the created fine mesh started at 0.1 mm on the wall and it was gradually increased. All four turbulent models were solved using the fine near wall mesh.

2) The standard wall functions (SWF): They are the default wall functions in Fluent and are based on the proposal of Launder and Spalding (1974). This approach is valid for full developed turbulent flow. The near wall mesh was fixed at 2 mm giving a y^+ between 6 and 25. Only the RNG turbulent model was tested with the two different wall approaches.

Additionally, the radiation heat on the cylinder surface was taken in account within the four turbulent models and the two wall approaches combinations. The RNG κ-ε model was also tested under zero radiation conditions. Table 1 summarizes all the different models characteristics.

Model	Turb.	Wall mesh	Wall App.	Rad
A	RNG κ-ε	Fine	EWT	Yes
B	RNG κ-ε	Coarse	SWF	Yes
C	Laminar	Fine	EWT	Yes
D	Std. κ-ε	Fine	EWT	Yes
E	SST κ-ω	Fine	EWT	Yes
F	RNG κ-ε	Fine	EWT	No

Table 1. Model characteristics

Boundary conditions

The inlet conditions for the different experimental trials are in Table 2.

At the tunnel outlet, zero normal gradients are assumed for all variables except pressure. At the walls of the tunnel, zero velocity, heat flux and water flux are assumed.

Exp	V (m/s)	Re.	T (K)	Tu.	RH (%)	P (Pa)
1	0.5	2759	293.26	2%	39.5	102103
2	1.5	8275	293.36	2%	39.8	102230
3	3	16531	293.76	2%	40.4	102070

Table 2. Inlet conditions

At the cylinder surface, both heat flux and water concentration change with the position around the cylinder. The mass transfer coefficient changes point by point depending of the development of the boundary layer. Thus, the heat flux, which depends of the evaporation rate, also changes around the surface. On the other hand, the mass flux at the surface depends on the wall water concentration gradient, which is calculated with the vapor pressure at the wall temperature. Thus, the concentration gradient is function of the wall temperature.

To establish the thermal and mass boundary conditions, conservation of heat and water equilibrium apply. There are two calculation procedures depending of the wall approach used.

Wall enhanced Treatment

In this case the mesh is fine enough and the mass flux in the interface can be calculated with the water concentration at the surface and in the cell next to the surface with the equation:

$$J_w = \rho D \frac{(Y_w - Y_c)}{ds} \quad (9)$$

The heat flux at the wall is calculated with the heat of vaporization and the radiation given the equation:

$$\dot{q}_w = J_w L_{vap} + \varepsilon\sigma\left(T_a^4 - T_w^4\right) \quad (10)$$

The water concentration in the interface is calculated point by point around the cylinder as a function of the surface temperature as follow:

1) The vapor pressure at the interface is calculated as a function of temperature using a vapor pressure–temperature equation.

2) The molar concentration is calculated from the relation between the vapor pressure and the total pressure.

3) The mass water concentration is calculated from the molar water concentration and the molecular weights.

Standard Wall Function

It was used in model B (modelling the turbulence with the RNG κ-ε model). In this case the surface mass flux was calculated with the equations proposed by Launder and Spalding (1974) assuming that species transport behaves analogously to heat transfer. The mass flux at the wall J_w is calculated from the equation:

$$Y^* = \frac{(Y_w - Y_c)\rho C_\mu^{1/4} \kappa_P^{1/2}}{J_w} = \begin{Bmatrix} Sc.y^* \quad for \quad \left(y^* < y_C^*\right) \\ Sc_t\left[\frac{1}{\kappa}\ln(E.y^*) + P_c\right] \; for\left(y^* < y_C^*\right) \end{Bmatrix} \quad (11)$$

Details of how calculate P_c, y_c^* and Sc_t are given in Fluent Inc. (2003). The heat flux at the wall and the water concentration at the surface are calculated in the same way as above.

Radiation effects

The heat of radiation was taken in account in modes A to E. Model F neglects the effect of radiation. Thus, equation 10 becomes:

$$\dot{q}_w = J_w L_{vap} \quad (12)$$

Boundary condition implementation

The thermal and mass boundary conditions are not constant and change point by point around the cylinder. They also depend on the solution of the other transport equation. Heat flux on the wall depends of the mass flux; surface water concentration depends on surface temperature. Therefore, both boundary conditions were established programming a Fluent UDF (User Defined Function). The Programmed UDF's are:

1) DEFINE_PROFILE(heat_vaporization, t, j): It calculates the heat flux leaving the cylinder interface caused by evaporation and radiation according to the equation 10. The calculation is done over each face element around the cylinder. The radiative term is excluded only on model F. The wall mass flux J_w was calculated with the equation 9 or 11 depending of the wall approach used.

2) DEFINE_PROFILE(water_interface, t, n): It calculates the surface water concentration as a function of temperature following the procedure explained under "Wall enhanced treatment". The calculation is also done over each face element around the cylinder.

Because it is necessary to know the concentration profile to start the calculation of the wall heat flux, the modelling is first done with constant boundary conditions. The wall temperature is fixed as the wet bulb temperature and the mass concentration as the calculated in equilibrium at the wet bulb temperature. After getting convergence, the above UDF's were activated and iterations started again until it converges. It was also necessary to use a relaxation factor of 0.1 in the water_interface UDF to get convergence.

RESULTS AND ANALYSIS

Table 3 shows the root mean square percentage error (%RMS) of the different models. The calculation was done comparing the experimental global mass flux $\bar{J}_w$ and temperatures with the corresponded values obtained by modeling. It is clearly seen that the model A gets the better experimental data fit. Figure 3 shows the experimental and calculated mass flux $\bar{J}_w$ using the models A to F. The enhanced wall function method gives better results than the standard wall function as can be seen comparing models A and B. This is because the wall functions were developed for full turbulent flows and not for low Reynolds numbers. The RNG κ-ε model gives slightly better results in the calculation of the mass flux than the standard κ-ε model (model D). That can be explained given the improvement in the RNG model that allows calculations at low Reynolds numbers. Model A gives the best result matching almost perfectly the experimental data.

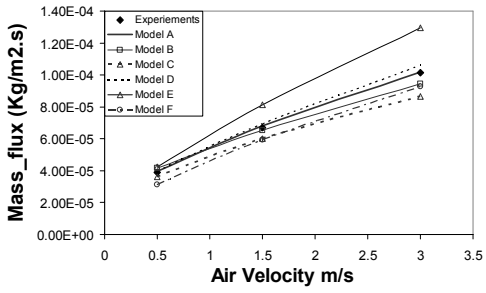

Figure 3. Mass flux vs. air velocity

Model	A	B	C	D	E	F
%RMS	0.51%	2.08%	7.41%	3.90%	7.15%	4.82%

Table 3. Global %RMS of the models.

Model	V =0.5	V=1.5	V=3	%RMS
Exp.	286.55	286.16	286.32	
A	286.65	286.32	286.38	0.03%
B	286.68	286.30	286.32	0.03%
C	286.81	286.43	286.45	0.07%
D	286.61	286.23	286.25	0.02%
E	286.57	286.11	286.13	0.04%
F	285.37	285.58	285.88	1.24%

Table 4. Temperature (K) vs. air velocity

Model	V =0.5	V=1.5	V=3	%RMS
Exp.	0.0104	0.0198	0.0307	
A	0.0107	0.0200	0.0312	1.48%
B	0.0111	0.0192	0.0292	4.51%
C	0.0095	0.0176	0.0261	10.38%
D	0.0108	0.0207	0.0332	5.00%
E	0.0115	0.0247	0.0416	22.38%
F	0.0106	0.0200	0.0313	1.51%

Table 5. $\overline{h}_m$ (Kg /m^{2}s) vs. air velocity

Model	V =0.5	V=1.5	V=3	%RMS
Exp.	9.22	17.94	28.53	
A	9.71	18.80	28.92	3.67%
B	10.52	17.74	26.15	8.20%
C	8.73	16.52	24.08	9.46%
D	9.68	18.93	29.60	4.18%
E	10.52	22.51	36.69	20.43%
F	9.76	18.81	28.90	3.87%

Table 6. $\overline{h}$ (W/m^{2}K) vs. air velocity

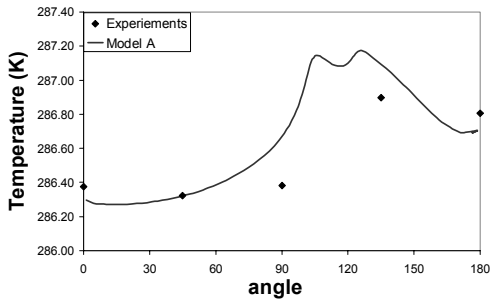

Figure 4. Temperature vs. angle at V = 0.5 m/s (model A)

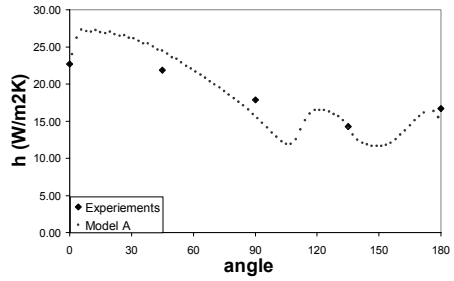

Figure 5. Local h vs. angle at V = 1.5 m/s (model A)

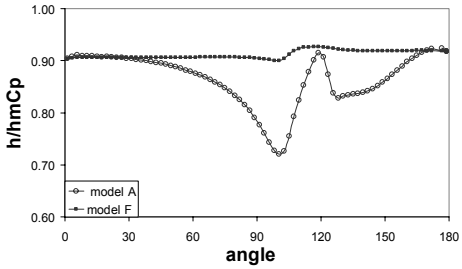

Figure 6. Relation $h / h_m C_P$ vs. angle at V = 0.5 m/s

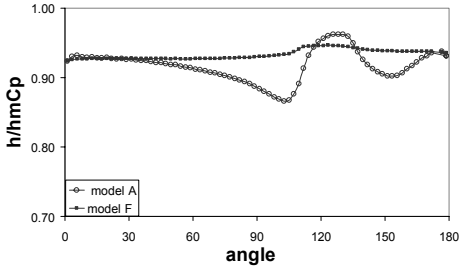

Figure 7. Relation $h / h_m C_P$ vs. angle at V = 1.5 m/s

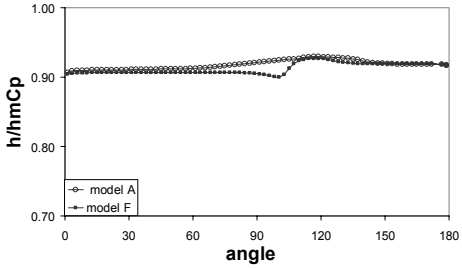

Figure 8. Relation $h / h_m C_P$ vs. angle at V = 3 m/s

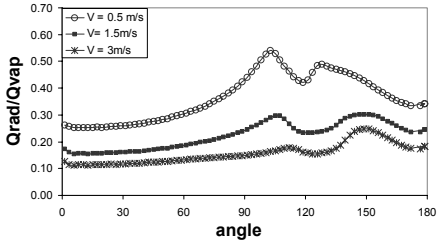

Figure 9. Relation Q_{rad}/Q_{vap} vs. angle

Although the SST κ-ω model (model E) was designed to be applied throughout the boundary layer, it did not fit the data better, as can be seen in Figures 3 and tables 4 to 6. The laminar model (model C) shows the lowest estimate of the mass flux, $\overline{h}$ and $\overline{h}_m$. That was caused because it did not take in account the effect of turbulence, which is important even though the turbulence intensity was just 2%.

Ignoring the effect of radiation (model F) causes underestimation of the mass flux (Figure 3) and temperature (Table 4). That can be explained with equation 10. Radiative heat is in opposite direction to evaporative heat flux and reduces the absolute value of the total wall heat flux. Thus, if radiation is not taken into account, the wall heat flux is higher and the wall

temperature is lower. Lower wall temperature means lower water surface concentration (given the dependence of temperature with vapour pressure), causing a lower water concentration gradient (or mass flux) in the wall.

The local prediction of temperature and h around the cylinder obtained with model A is good as it can be seen in Figures 4 and 5 (the angle is taken from the stagnant point).

The relationship between the global heat and mass transfer coefficients ($\bar{h}/\bar{h}_m C_p$) is almost constant and close to the value of $L_e^{2/3} \approx 0.892$ agreeing with the Chilton-Colburn analogy (Equation 5). However, there were differences found in the local relationship ($h/h_m C_p$) at low velocities when the radiative heat was taken in account. Figures 6, 7 and 8 show the local relationship between the heat and mass transfer coefficient as a function of the angle using models A and F. Figure 6 (made at V = 0.5 m/s) shows that using model A the relationship strongly deviates from a constant value reaching a minimum (19% deviation) at the separation point of the boundary layer. If the radiative heat is not taken in account (model F) the relation is constant and very close to $L_e^{2/3}$ as in Equation 5. The deviation decreases when the air velocity increases (figures 7 and 8), almost getting a constant value at V = 3 m/s. Figure 9 shows that the radiative heat becomes less important compared with the evaporative heat at higher air velocities. The deviation of the Chilton-Colburn equation at low velocities, or low Reynolds numbers, seems to be influenced by the heat of radiation that becomes important at low air velocities. That effect is stronger at the detachment of the boundary layer where the heat transfer coefficient is decreasing while the mass transfer coefficient is increasing, causing the ratio heat to mass transfer coefficients to decrease. At this point, the convection effects decrease and the radiation effect becomes more important causing the surface temperature to rise (Figure 4). The normal temperature gradient decreases making the wall heat flux reduce. Therefore, the local heat transfer coefficient decreases. Cess (1962) analytically shows that the local Nusselt number (non-dimensional heat transfer coefficient) in a laminar boundary layer of a fluid along a flat plate decreases by effect of radiation. The effect of radiation on the mass transfer coefficient is opposite to heat transfer coefficient. It makes the mass transfer coefficient to increase. This is because the wall temperature increases, as it was established above, making the vapour pressure and the water composition on the wall to increase. This increment on the wall water composition makes the mass gradient at the wall to rise and therefore, the mass transfer coefficient increases. This work shows that the Chilton-Colburn analogy loses accuracy to relate the local heat and mass transfer coefficients at low air velocities. The accuracy of this analogy (Equation 5) to correlate heat and mass transfer coefficients on evaporation and drying processes has been questioned before (Chen *et all* (2002))

CONCLUSION

1) The psychrometric method of Kondjoyan and Daudin (1993b) was followed to experimentally determine local and global heat and mass transfer coefficients around a cylinder at Reynolds numbers between 2700 and 17000.

2) The experiments were modelled with different turbulence models and two wall treatment approaches. It was found that the RNG κ-ε model using the enhanced wall treatment and taking in account the effect of radiation fits better the experimental data.

3) The CFD modelling shows that at low Reynolds numbers when the radiative heat is taken in account the relation $h/h_m C_P$ is not constant around the cylinder, reaching a minimum value at the detachment of the boundary layer.

ACKNOWLEDGEMENTS

The authors whish to acknowledge the support of the Australian Government through the Australian Research Council Large Grant A00103716.

REFERENCES

CESS, R. D., (1962), "The effect of radiation upon forced-convection heat transfer", Appl. Sci. Res., Section A, **10**, 430-438,.

CHEN X. D., LIN S. X. Q. and CHEN G., (2002), "On the ratio of heat to mass transfer coefficient for water evaporation and its impact upon drying modelling". Int. J. Heat and Mass Transfer, **45**, 4369-4372.

FLUENT INC., (2003), Fluent 6.1.18 user's guide, Vols. 1-5, Fluent Inc., Lebanon NH USA.

KESTIN J. and WOOD R. T., (1971), "The influence of turbulence on mass transfer from cylinders", J. Heat Transfer, **93**, 321—327.

KONDJOYAN, A. and DAUDIN, J.D., (1993a), "Heat and Mass Transfer Coefficients at the surface of Elliptical Cylinders placed in a Turbulent air flow", J. of Food Eng., **20**, 339-367.

KONDJOYAN, A. and DAUDIN, J.D., (1993b), "Determination of transfer coefficients by psychrometry", Int. J. Heat Mass Transfer, 36, No. **7**, 1807-1818.

KONDJOYAN, A. and DAUDIN, J.D., (1997), " Heat and Mass Transfer-Coefficients at the surface of a Pork Hindquarter", J. of Food Eng., **32**, 225-240.

LAUNDER, B.E. and SPALDING, D.B., (1974), 'The numerical computation of turbulent flows", Computer Methods in Applied Mechanics and Engineering, **3**, 269-289.

LEWIS J. S., (1971), "Heat transfer predictions from mass transfer measurements around a single cylinder in cross-flow", Int. J. Heat and Mass Transfer, **14**, 325-329.